3
Control strategies

As the objective of the work in this thesis is to reduce torsional vibrations and eliminate the stick-slip, the designed controller is projected to maintain a desired constant angular velocity ω_d for the entire drill-string. So, the objective when designing a controller for this kind of system is to regulate the nonlinear drillstring with frictions system to a desired setpoint ω_d using a designed controller.

The measurements available with a good precision for the controller are the top drive angular velocity ω_{td} and the reactive torque on the top drive T_{TD}, which implies that only surface measurements can be implemented as state feedback. The system, on a real drilling problem can be controlled by the top drive torque T_{TD}. The controller should be designed in a way that it:

1. Locally stabilizes the rotational velocity of the drill-string, eliminating torsional vibrations, specially stick-slip.

2. Ensures robustness with respect to uncertainties in the nonlinear bit-rock interaction, time delays on measurements, and unmodeled dynamics of the system.

3. Guarantees the satisfaction of closed-loop performance specifications, considering the dynamical limitation of the actuators.

3.1 PID control

The most widely used type of control is the proportional-integral-derivative (PID) control. This controller is widely applied due to its simplicity, ease of implementation and for the characteristics of being easy to tune without modeling the plant, only by observing the behavior of the plant and adjusting 3 gains until de desirable result is obtained. A PID controller continuously calculates an error value $e(t)$ as the difference between a desired setpoint $r(t)$ and a measured process variable $y(t)$ and applies a correction based on proportional, integral, and derivative terms. The controller attempts to minimize the error over time by adjustment of a control variable $u(t)$, to a new value determined by a weighted sum given by

$$u(t) = K_p e(t) + K_i \int_0^t e(t)dt + K_d \frac{d}{dt} e(t) \tag{3.1}$$

where K_p, K_i and K_d, are non-negative scalars that denote the coefficients for the proportional, integral, and derivative gains. Figure (3.1) shows the block diagram implementation of the PID structure.

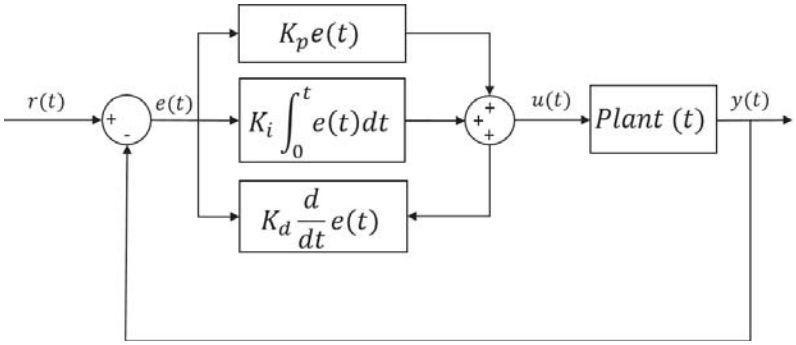

Figure 3.1: PID Control closed loop structure

In addition of the trial and error method for tuning the PID gains, some other mathematical methods can be used of optimum tuning of the system based on the knowledge of the plant model. One of the most famous methods is the Ziegler-Nichols. Todays simulation softwares have many methods for tuning ready for use.

The main limitation of the PID is that it is a linear control and it has bad results on time varying plants and in the presence of time delays. Other limitation is that it has constant gains, so in the presence of plant changes, unmodeled dynamics, delays, uncertainties, etc., this control looses its efficiency and in most cases cannot stabilize the system.

3.2 Adaptive control

A system considered adaptive is the one capable of maintaining its performance and stability despite of changes in the environment, on its own parts and in the presence of uncertainties. This is valid for a variety of systems, not only in engineering but systems in nature, population and social patterns, living organisms, etc. The maintenance of the good performance of the system in the presence of large changes of either the systems environment or the system itself is named adaptation in the control systems literature.

In all cases, adaptive systems are by essence nonlinear, as they have parameters that are functions of their states. Thus, adaptive systems are simply a special class of nonlinear systems that measure their own performance, operating environment, and operating condition of components, and adapt their dynamics, or those of their operating environments to ensure that measured performance is close to targeted performance or specifications.

Adaptive control differs from robust control by the fact that it does not need a priori information about the bounds on these uncertain or time-varying parameters. Robust control on the other hand, guarantees that if the changes are within given bounds the control law need not be changed, while adaptive control is based in the control law changing itself.

The first steps in the use of adaptive control theories were due to the advances in the aerospace industry during the 1950s in an attempt to improve the design of autopilots [7]. The control theories known in those years were not able to satisfy the requirements for the new aircrafts that were being designed. After the successful implementation of jet engines into aircraft, flight envelopes largely increased resulting in a wide range of operating conditions for a single aircraft. Flight envelopes grew even more with developing interest in hypersonic vehicles from the community. The existing autopilots at the time left much to be desired in the performance across the flight envelope, and engineers began experimenting with methods that would eventually lead to Model Reference Adaptive Control (MRAC).

In the early developments of MRAC control architectures the notion of stability in the feedback loop and in adaptation was not well understood or as mature as today and that, combined with the limited capabilities of on board computers put in doubt the effectiveness of MRAC models, especially after some accidents with test airplanes.

The late 1950s and early 1960s saw the formulation of the state-space system representation as well as the use of Lyapunov stability for general control systems, by both Kalman and Bertram [22] [23]. Aleksandr Lyapunov first published his book on stability in 1892, but the work went relatively unnoticed (at least outside Russia) until the 1960's. It has since then been the main tool used for general system stability and adaptation law design. The first MRAC adaptation law based on Lyapunov design was published by Parks in 1966 [1]. During this time Filippov, Dubrovskii and Emelyanov were working on the adaptation of variable structure systems, more commonly known as sliding mode control [46].

Adaptive Pole Placement, often referred to as Self-Tuning Regulators, were also developed in the 1970s by Astrom and Egardt with many successful applications [6] [8], with the added benefit of application to non-minimum phase systems.

Recent developments in adaptive control from 2000s until today, are a little controversial. From 2006 to 2011 it was presented to the community in conferences and papers the creation of the L_1 adaptive control method [12] [13] [15] [11] [16] [17] which garnered a lot of excitement and widespread

implementation including some very important applications in the aerospace industry for several years. Some of the advantages of the method included: decoupling adaptation and robustness, guaranteed fast adaptation, guaranteed transient response without persistent excitation, and guaranteed time-delay margin.

In 2014, Ioannou et.al. [19] reviewed some of the assumptions of L_1 control. It analyses if the L_1 adaptive controller provides improvements over the pre-existent MRAC schemes by analysing a simple plant with all states observed. His analysis shows that the insertion of the proposed low-pass filter deteriorates the performance and robust stability margin bounds when compared to standard MRAC. In the authors words: "The use of high adaptive gains recommended in the L_1 approach may cause two major problems. First, it makes the differential equation of the adaptive law very stiff leading to possible numerical instabilities. Second, it makes the adaptive scheme less robust with respect to unmodeled dynamics". However, the analysis made by this author was not done in the general formulation of the L_1 adaptive controller. Instead, he analyzed a controller that is a standard MRAC with a low pass filter. The author misses the point that in L_1 control architectures, the filtered control signal is sent to both the plant and the state predictor, the filter is thus embedded into the adaptive architecture, which implies that one cannot analyze the closed-loop system as if the adaptive controller and the filter were acting in series.

Ortega and Panteley [31] stated, in the title of the article that: L_1 Adaptive Control Always Converges to a Linear PI Control and Does Not Perform Better than the PI (in authors words). In the article, it is said that the L_1 controller coincides with a full-state feedback, linear time-invariant proportional plus integral (PI) controller with a decaying additive disturbance. It is also shown in the article that if the PI controller does not stabilize the plant the L_1 adaptive controller will not stabilize it either. The assumptions made in this article are in part true, but this convergence to a linear PI control only occurs in a very specific and limited set of applications. As the problem analyzed in this thesis is not related to the ones presented by [31], this will not affect the implementations of L_1 in this thesis.

Naira Hovakimyan, in a response letter published in her website [1], addressed many of the questions posed to the L_1 adaptive control. In this article, it is shown that the bandwidth-limited low pass filter C(s) must be placed in the correct point of the L_1 controller architecture to properly decouple the estimation loop from the control loop, which is critical to allow to increase the adaptation gain without compromising the robustness margins. It is also

shown that the time delay margins of the L_1 adaptive controller is much better than the one from the MRAC controller when the adaptation gain is increased. For large adaptation gains the MRAC controller time delay margin tends to zero.

In 2014 Hsu [18] proposed a combination of two known methods that share common features with L_1 control (Smooth sliding control and Binary model reference adaptive control) as a solution to overcome some limitations of the L_1 adaptive control, this method was named extended binary model reference adaptive control.

From the above mentioned articles, it was concluded that the problems and limitations of the L_1 adaptive controller presented in literature does not affect in a negative way the implementation of this control architecture for the torsional dynamics of the drillsting model, object of this thesis.

Most of the confusion and reports of bad results with the L_1 adaptive control comes from the fact that there are some small differences on the architecture of the L_1 adaptive controller depending on the type of model one is trying to control. In this thesis only one architecture is presented, the one adequate to control the output feedback models used.

3.3 MRAC control

Within all the adaptive controller types, the most used by far is the Model Reference Adaptive Control (MRAC). The basic structure of a MRAC scheme is shown in Fig. (3.2).

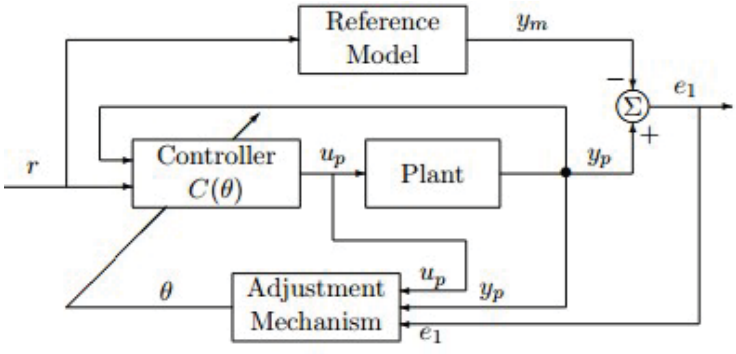

Figure 3.2: MRAC Controller scheme

The goal of the designed reference model is to generate the desired trajectory, y_m, that the plant output y_p has to follow. The tracking error $e_1 = y_p - y_m$ represents the deviation of the plant output from the desired trajectory. The closed-loop plant is made up of a common feedback control law that contains the plant and a controller $C(\theta)$; an adjustment mechanism

that generates the controller parameter estimates $\theta(t)$ on-line. The objective is to design the controller and parameter adjustment mechanism so that all signals in the closed-loop plant are bounded and the plant output y_p tracks y_m as close as possible.

Equation 3.2 represents the dynamical behavior of the system in the form of a differential equation.

$$\begin{aligned} \dot{x}(t) &= A_m x(t) + b(u(t) + k_x^T x(t)), \qquad x(0) = x_0, \\ y(t) &= c^T x(t), \end{aligned} \tag{3.2}$$

where $x(t)$ is the state of the system (measured), A_m is the state matrix of the system, b and c are known constant vectors, k_x is a vector of unknown constant parameters, $u(t)$ is the control input, and $y(t)$ is the regulated output. The objective is to define an adaptive feedback signal $u(t)$ such that $y(t)$ tracks $r(t)$ with desired specifications, while all the signals remain bounded.

The controller is given by:

$$u(t) = -\hat{k}_x^T(t)x(t) + k_g r(t) \tag{3.3}$$

where k_g ensures that $y_m(t)$ tracks step reference inputs with zero steady-state error. The hat over a term indicates an estimate of it.

And the update law is given by:

$$\dot{\hat{k}}_x(t) = -\Gamma x(t)e^T(t), \qquad \hat{k}_x(0) = k_x(0) \tag{3.4}$$

where Γ is the adaptation gain.

As explained in details in [16] from the MRAC control law and the adaptive laws, it follows that large adaptive gains result in high-gain feedback control, which manifests itself in high-frequency oscillations in the control signal and reduced tolerance to time delays. Moreover, applications requiring identification schemes with time scales comparable with those of the closed-loop dynamics appear to be extremely challenging due to undesirable interactions of the two processes. Due to lack of systematic design guidelines to select an adequate adaptation gain, tuning of such applications is being commonly resolved by either computationally expensive Monte Carlo simulations or trial-and-error methods following some empirical guidelines and intuition. As a consequence, proper tuning of MRAC architectures represents a major challenge and has largely remained an open question in literature.

3.4 L_1 adaptive control

The L_1 adaptive control structure key idea is to enable fast adaptation with guaranteed robustness to overcome one of the main limitations of MRAC control structure. A simple stable scalar system with constant disturbance can be used to highlight the advantages of L_1 control, specially showing how the fast adaptation of the L_1 controller actually improves the system robustness. Considering the scalar system:

$$\dot{x}(t) = -x(t) + \theta + u(t), \qquad x(0) = x_0 \tag{3.5}$$

where θ is the unknown constant acting as undesired perturbation, and $u(t)$ is the control input. For this system a general MRAC architecture reduces to an integral controller of structure

$$u(t) = -\hat{\theta}(t) = -\hat{k_x^T} x(t) \tag{3.6}$$

where $\hat{\theta}(t)$ is the estimate of θ given by

$$\dot{\hat{\theta}}(t) = -\Gamma(x_m(t) - x(t)), \qquad \theta(0) = \theta_0, \qquad \Gamma > 0 \tag{3.7}$$

and $x_m(t)$ is the reference signal. One can notice that this reference system is obtained from the original system (3.5) by substitution of the ideal nonminimal controller $u_{nom}(t) = -\theta$ into it, assuming then a perfect cancellation of the uncertain parameter θ in the system.

The negative feedback loop transfer function of this system is

$$L_1(s) = \frac{\Gamma}{s(s+1)} \tag{3.8}$$

As the closed-loop system (3.8) remains linear time-invariant (LTI), it is possible to use standard classical control tools to analyze its stability margins. The two most commonly used stability margins are the gain and the phase margin. As the Nyquist of $L_1(s)$ never crosses the negative part of the real axis, the closed-loop system has infinite gain margin ($gm = \infty$) and the gain crossover frequency ω_{gc} can be computed from

$$|L_1(j\omega_{gc})| = \frac{\Gamma}{\omega_{gc}\sqrt{\omega_{gc}^2 + 1}} = 1 \tag{3.9}$$

and the system phase margin

$$\phi_m = \pi + \angle L_1(j\omega_{gc}) = arctan\left(\frac{1}{\omega_{gc}}\right) \tag{3.10}$$

An inspection indicates that increasing Γ leads to higher gain crossover frequency and consequently reduces the phase margin, so, if increasing Γ

improves the tracking performance for all $t \geq 0$, including the transient phase, it compromises the robustness (or relative stability) of the closed-loop system. Thus, the adaptation rate Γ is the key to the trade-off between performance and robustness. Since tracking and robustness cannot be achieved simultaneously using this architecture, the goal is to explore if the architecture can be modified so that the trade-off between tracking and robustness is resolved differently and the adaptation gain Γ can be safely increased for transient performance improvement without compromising the robustness of the closed-loop system.

To obtain the L_1 adaptive controller for this system, the controller in (3.6) and (3.7) will be modified in two ways. First, we add the state predictor

$$\dot{\hat{x}}(t) = -\hat{x}(t) + \hat{\theta}(t) + u(t) \qquad \hat{x}(0) = x_0 \tag{3.11}$$

which leads to the following prediction error dynamics, independent of the control choice

$$\dot{\tilde{x}}(t) = -\tilde{x}(t) + \tilde{\theta}(t) \qquad \tilde{x}(0) = x_0 \tag{3.12}$$

where $\tilde{x}(t) = \hat{x} - x(t)$ and $\tilde{\theta}(t) = \hat{\theta}(t) - \theta$. The parametric estimate, given by (3.7), is then substituted by

$$\dot{\hat{\theta}}(t) = -\Gamma\tilde{x}(t), \qquad \theta(0) = \theta_0, \qquad \Gamma > 0 \tag{3.13}$$

Then, the adaptive controller written as $u(t) = -\hat{\theta}(t)$, is replaced by a new version of $\hat{\theta}(t)$ with a low-pass filter $C(s)$.

$$u(s) = -C(s)\hat{\theta}(s) \tag{3.14}$$

where $u(s)$ and $\hat{\theta}(s)$ are the Laplace transforms of $u(t)$ and $\hat{\theta}(t)$ respectively, and C(s) is a bounded-input bounded-output (BIBO) stable strictly proper transfer function subject to $C(0) = 1$ with zero initialization for its state-space realization. Figure 3.3 shows the closed-loop block diagram of this system.

Considering the first order low pass filter $C(s)$

$$C(s) = \frac{\omega_c}{s + \omega_c} \tag{3.15}$$

and the negative feedback loop transfer function

$$L_2(s) = \frac{\Gamma C(s)}{s(s+1) + \Gamma(1 - C(s))} \tag{3.16}$$

one can notice that in the case where there is no filter $C(s)$, the L_1 controller becomes a conventional MRAC type integral controller. From (3.8), i.e. $L_2(s) = L_1(s)$.

The phase and the gain margins of the L_1 controller are not significantly affected by large values of Γ. While the phase margin of the MRAC type

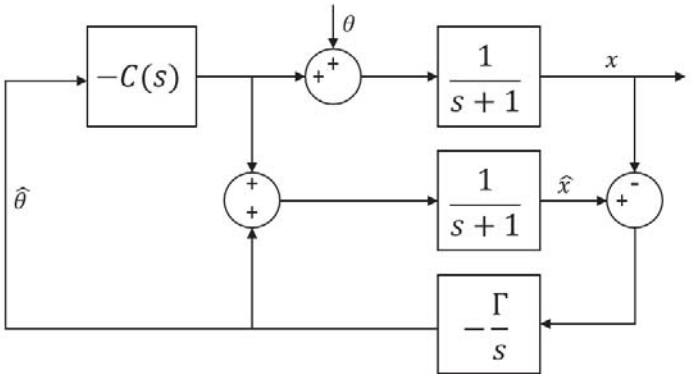

Figure 3.3: L_1 Control closed loop structure

integral controller vanishes as the adaptation gain Γ is increased, the L_1 adaptive controller has a guaranteed bounded away from zero phase and gain margins in the presence of fast adaptation.

One can also notice that as $\Gamma \to \infty$ the expression in (3.16) leads to the following loop transfer function

$$L_2(s) = \frac{C(s)}{1 - C(s)} = \frac{\omega_c}{s} \tag{3.17}$$

This loop transfer function gain margin converges to $gm = 6.02dB$ when $\Gamma \to \infty$ and a phase margin of $\phi_m \to \pi/2$. One can also notice that the high-frequency dynamics of the adaptation loop does not appear in the limiting loop transfer function.

3.5 L_1 control formulation

Considering a single input single output (SISO) system in the form:

$$y(s) = A(s)(u(s) + d(s)) \tag{3.18}$$

where $u(s)$ is the Laplace transform of the systems input signal $u(t)$; $y(s)$ is the Laplace transform of the systems output signal $y(t)$; $A(s)$ is a strictly proper unknown transfer function and $d(s)$ is the Laplace transform of the uncertainties and disturbances.

This system in (3.18) can be rewritten in terms of the reference system, defined by $M(s)$, as:

$$y(s) = M(s)(u(s) + \sigma(s)) \tag{3.19}$$

where the uncertainties due to $A(s)$ and $d(s)$ are lumped into the signal $\sigma(s)$:

$$\sigma(s) = \frac{(A(s) - M(s))u(s) + A(s)d(s)}{M(s)} \tag{3.20}$$

Another important step into calculating the design of the L_1 adaptive controller is to calculate a strictly proper low pass filter $C(s)$ respecting $C(0) = 1$ in the form:

$$H(s) = \frac{A(s)M(s)}{C(s)A(s) + (1 - C(s))M(s)} \tag{3.21}$$

such that $H(s)$ is stable, and the L_1-norm condition holds:

$$||G(s)||_{L_1} L < 1 \tag{3.22}$$

where

$$G(s) = H(s)(1 - C(s)) \tag{3.23}$$

The output predictor is written in the form:

$$\dot{\hat{y}}(t) = -m\hat{y}(t) + m(u(t) + \hat{\sigma}(t)) \tag{3.24}$$

where $\hat{y}(0) = 0$ and $\hat{\sigma}(t)$ is the adaptive estimate. The adaptation law of $\hat{\sigma}(t)$ is:

$$\dot{\hat{\sigma}}(t) = \Gamma Proj(\hat{\sigma}(t), \tilde{y}(t)) \tag{3.25}$$

where $\hat{\sigma}(0) = 0$ and $Proj$ is the projection operator.

Which leads to the following L_1 architecture:

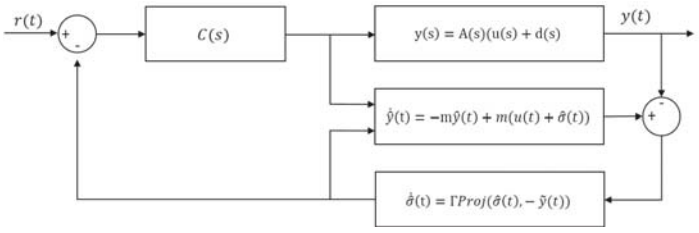

Figure 3.4: Closed loop L_1 architecture

As described in [47], the selection of $C(s)$ and $M(s)$ must ensure that

$$H(s) = \frac{A(s)M(s)}{C(s)A(s) + (1 - C(s))M(s)} \tag{3.26}$$

is stable, and that the L_1 gain of the system is upper bounded as:

$$||H(s)(1 - C(s))||_{L_1} < 1 \tag{3.27}$$

where $C(s)$ is a low pass filter with DC gain $C(0) = 1$.

3.5.1 L_1 Control simulation results

In order to better understand the implementation of the L_1 control, the two cart model was simulated with an adaptive L_1 controller.

The two cart problem (fig. 3.5), was originally proposed as a benchmark to analyze the results of robust control theories. This model, that is a more complex version of the one cart mass-spring-damper model, will be used in to test and benchmark the proposed L_1 controller, as it is used in literature [16] to analyze the results of adaptive controllers.

As the L_1 adaptive control is a new formulation that present some difficulties in the implementation, it was chosen to initially implement a model (two cart) that has simulations presented by the authors of the control law in order to evaluate the MatLab code of the control before implementing it on the rotational system, core of this thesis.

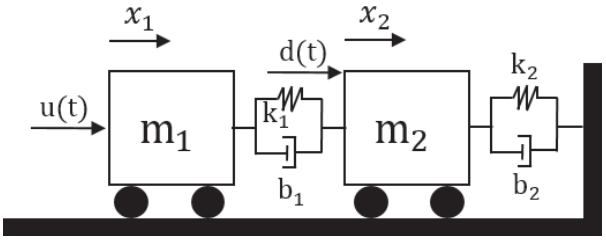

Figure 3.5: Two cart mass spring damper system

The dynamics of this system can be written in a state space form by:

$$A = \begin{bmatrix} 0 & 0 & 1 & 0 & 0 \\ 0 & 0 & 0 & 1 & 0 \\ \frac{-k_1}{m_1} & \frac{k_1}{m_1} & \frac{-b_1}{m_1} & \frac{b_1}{m_1} & 0 \\ \frac{-k_1}{m_2} & -\frac{k_1+k_2}{m_2} & \frac{b_2}{m_2} & -\frac{b_1+b_2}{m_2} & \frac{1}{m_2} \end{bmatrix} \quad B = \begin{bmatrix} 0 \\ 0 \\ \frac{1}{m_1} \\ 0 \end{bmatrix} \quad x = \begin{bmatrix} x_1(t) \\ x_2(t) \\ \dot{x_1}(t) \\ \dot{x_2}(t) \end{bmatrix} \tag{3.28}$$

Where the states $x_1(t)$ and $x_2(t)$ represent the positions of the two carts, whose respective masses are m_1 and m_2, respectively but in this problem only $x_2(t)$ is measured, $d(t)$ is a normally distributed random disturbance force acting on the mass m_2, $u(t)$ is the control force, which acts upon the mass m_1, and α is a constant that multiplies the disturbance.

The complete state space matrices are written in the form:

$$\dot{x} = Ax + Bu \tag{3.29}$$

where u is the input vector.

This classical benchmark problem has been modified to insert a friction between mass m_2 and a moving belt in order to create a stick-slip behavior on mass m_2 although the control input force $u(t)$ still acts on mass m_1.

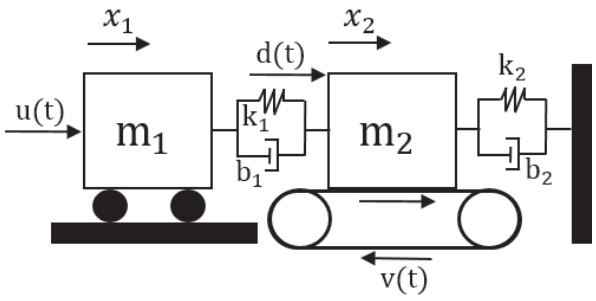

Figure 3.6: Two cart mass spring damper system with friction on m_2

Equations of motion for this system in the state space form can be obtained by adding the friction laws 2.16 and 2.17 to the state space representation of the two cart model 3.28. This system was then simulated with the flowing conditions:

$$m_1 = m_2 = 1kg, \quad k_1 = k_2 = 0.15N/m, \quad b_1 = b_2 = 0.1N/m/s, \quad \alpha = 0.1 \tag{3.30}$$

Those values are the same ones used in [17] and [20] to test the response of adaptive controllers.

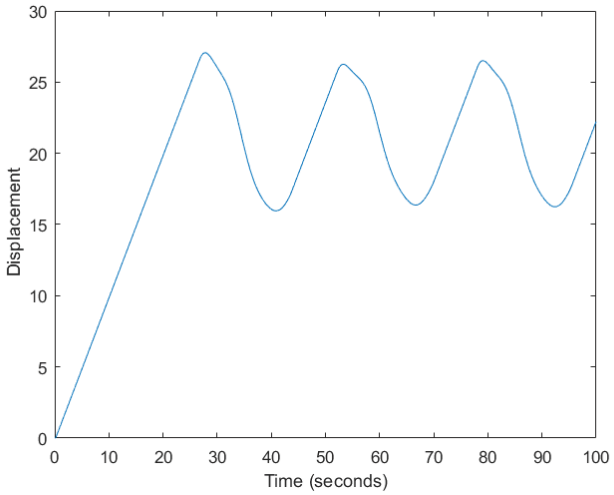

Figure 3.7: Displacement of the cart m_2 of the mass spring damper system with dry friction on m_2

Figure 3.7 shows the displacement over time for this system, where the belt under mass m_2 moves at a constant speed of $1m/s$. This simulation is performed to show that the known robust control benchmark problem can be modified to have a stick-slip behavior and test the effectiveness of a given

control law to mitigate the stick-slip on this simple problem. The results for an adaptive controller will be presented in chapter 3.

In this system the belt is moving with constant speed and the control aims to place the mass m_2 in the reference position $r(t)$ by actuating on the mass m_1. $d(t)$ is a disturbance force acting on mass m_2 For this simulation, the reference model is a third order system whose respective transfer function is shown in eq. (3.31). This transfer function is obtained from the system described in eq. 3.28 with the parameters from eq. (3.30).

$$M(s) = \frac{1}{s^3 + 1.4s^2 + 0.17S + 0.052} \tag{3.31}$$

And the low pass filter used in the control law:

$$C(s) = \frac{0.18s + 0.19}{s^5 + 2.8s^4 + 3.3s^3 + 2.0s^2 + 0.66S + 0.19} \tag{3.32}$$

This $C(s)$ filter is a low pass filter, with cutoff frequency of $0.4rad/s$ as described in section 3.4 and its bode plot:

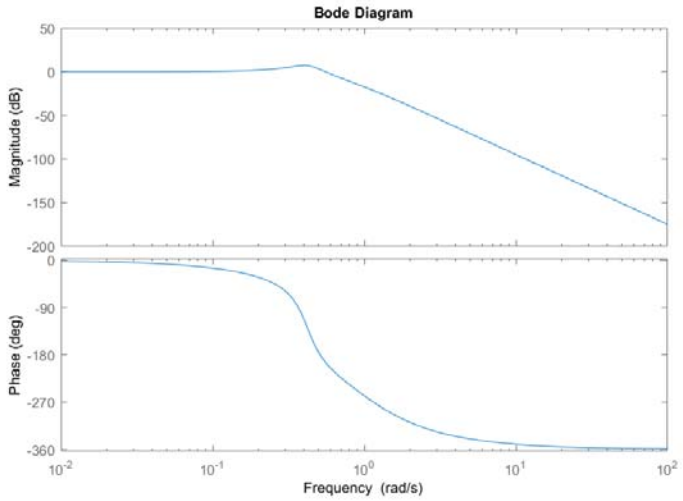

Figure 3.8: $C(s)$ filter bode plot

Figures 3.9 and 3.10 show the result of the L_1 controller in comparison with the open loop system that is subjected to the stick-slip due to the moving belt under the mass m_2. The reference signal $r(t)$ in this case was 0, the displacements observed in fig. 3.9 are caused only by the friction force with the belt, and the displacements on the system with L_1 (fig. 3.10) are caused by this same friction but in this case, also by the control force $u(t)$.

The control effort in this simulation is shown in fig. 3.14:

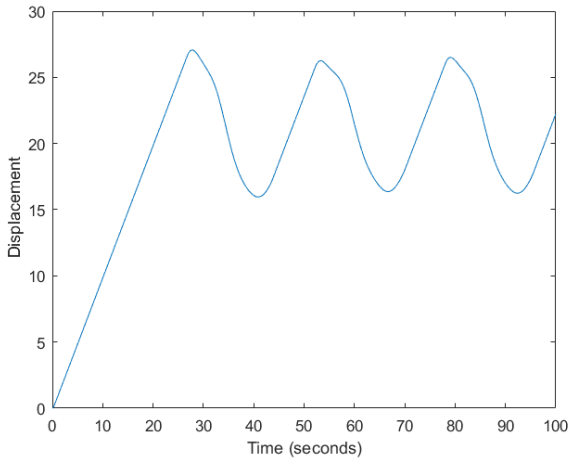

Figure 3.9: Displacement of the cart m_2 without control

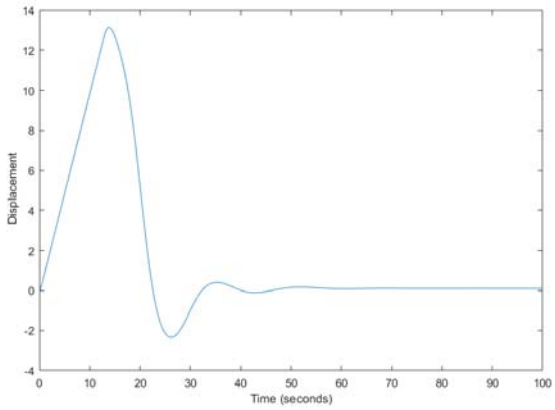

Figure 3.10: Displacement of the cart m_2 with L_1 control

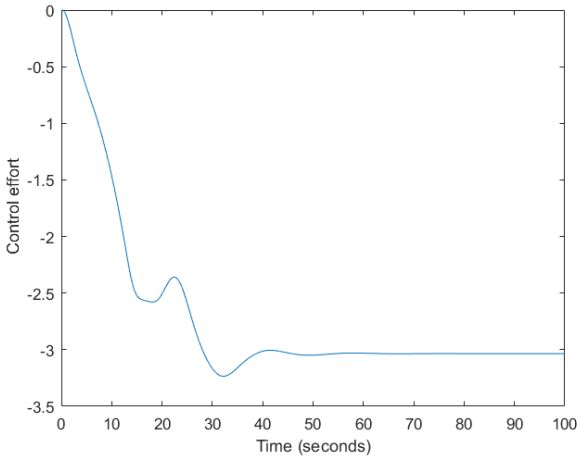

Figure 3.11: Control effort of the L_1 controller

Which complies with the expected behavior in this case, that is, after the system is stabilized by the controller adaptation, the steady state becomes almost constant, applying on the system the force needed to compensate the dynamical friction force of the belt.

To test the controller performance in the presence of unmodeled disturbances, the same simulations were performed adding a disturbance force $d(t)$ modeled as normally distributed random force of power = 0.01.

Figures 3.12 and 3.13 show the result of the L_1 controller in comparison with the open loop system both with the disturbance force on the mass m_2. The reference signal $r(t)$ in this case was 0, the displacements observed in fig. 3.12 are caused only by the friction force with the belt and the disturbance, and the displacements on the system with L_1 (fig. 3.13) are caused by this same friction and disturbance but in this case, also by the control force $u(t)$.

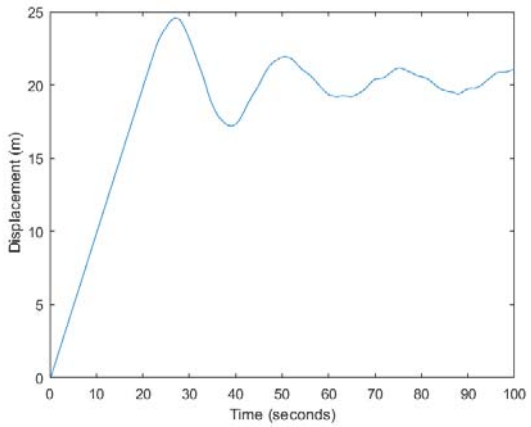

Figure 3.12: Simulation results for the 2 DOF linear system: Displacement of the cart m_2 without control

The control effort in this system is shown in fig. 3.14.

Continuing this analysis, the response of the L_1 controller is analyzed for a non constant reference signal $r(t)$. The displacement of mass m_2 and the reference signal $r(t)$ are shown in fig. 3.15.

The control effort in this system is shown in fig. 3.16.

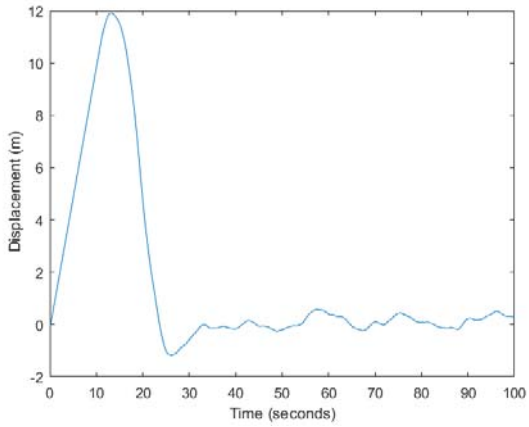

Figure 3.13: Simulation results for the 2 DOF linear system: Displacement of the cart m_2 with L_1 control

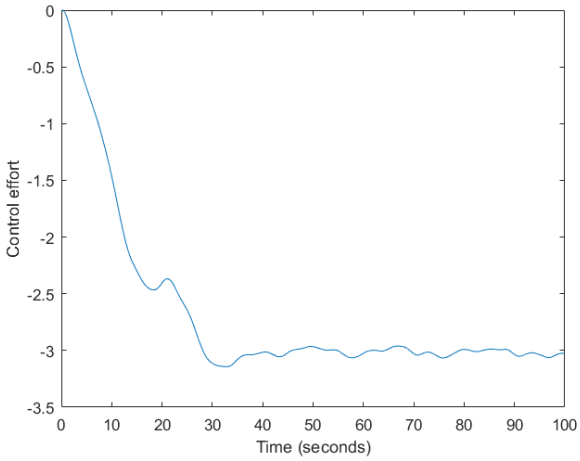

Figure 3.14: Control effort of the L_1 controller

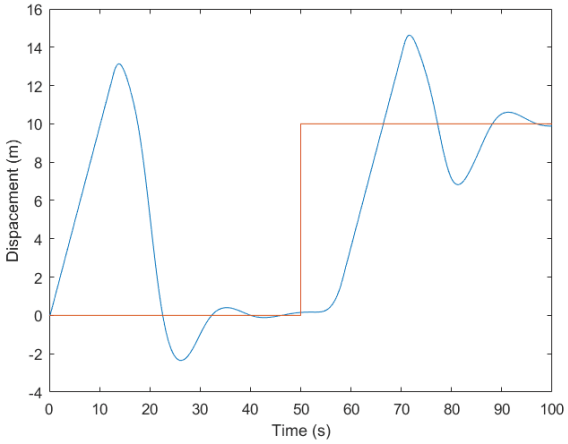

Figure 3.15: Displacement of m_2 (blue) and reference signal $r(t)$ (orange)

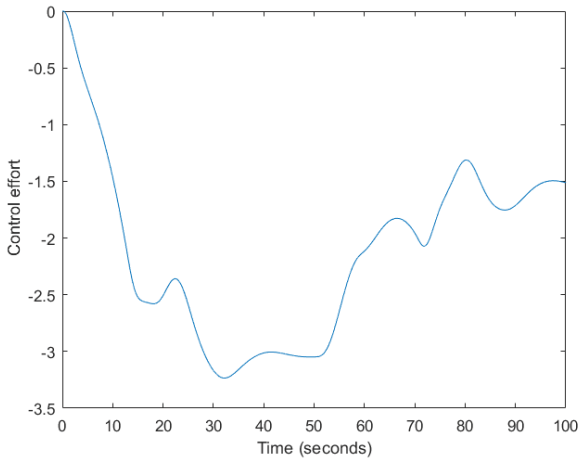

Figure 3.16: Control effort of the L_1 controller

As one can see, the proposed L_1 control shows good results for the two cart example in the presence of unmodeled contact with a moving belt under m_2.

3.6 L_1 augmented PID control

L_1 augmented PID control is a closed loop control that tries to combine the good results that can be achieved using a well tuned PID control (Section 3.1) on linear systems with the adaptiveness and robustness of the L_1 control (Section 3.4). This way, it is possible to obtain a fast response system based on PID that can overcome the PID limitations, being able to tolerate non modeled dynamics, time delays, sensor noises, etc.

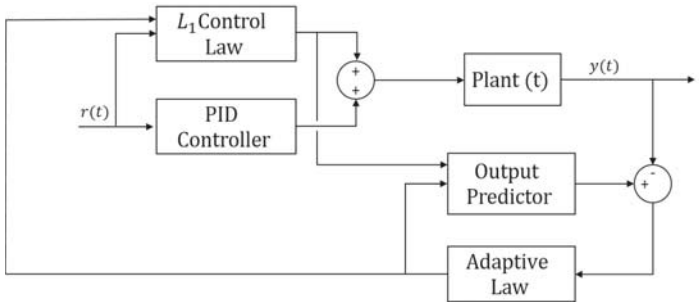

Figure 3.17: L_1 augmented PID control structure

In this strategy, we tune a PID controller to a reference system without delays and disturbances, then we project the L_1 adaptive control in order eliminate every possible unknown disturbances and delays, bringing the system to the known configuration used to tune the PID.

As the main advantage of the L_1 controller is to enable an increase of the adaptation rate without compromising the robustness of the system as stated in section 3.4, one can say that, theoretically, it should be possible to increase the adaptation gain Γ until the desired response in achieved. That would be possible, but the limitation imposed on the design of this simulations was to have a discrete control loop with a loop time of $10ms$ as this is a achievable target for normal control hardwares. This way, our goal is to design a system that can be implemented for a real laboratory reduced scale test rig.

In order to test the advantages of the proposed L_1 adaptive control applied to the investigated drilling problem, a time delay of 20ms was added on the angular speed of J_1 measurement shown in fig. 3.18

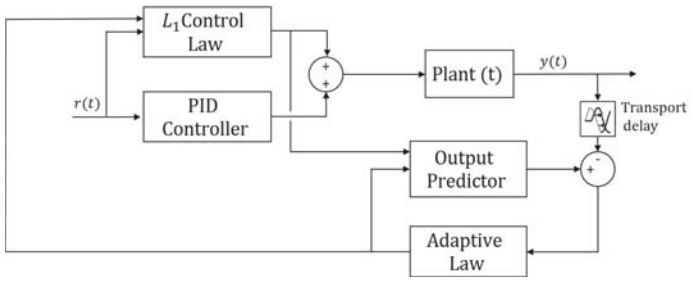

Figure 3.18: L_1 augmented PID control structure with time delay

It was also added as disturbance, a second point of dry friction, with the same mathematical modeling as the one acting on the inertia J_1 but with the applied torques for each speed being half of the ones acting on J_1. This disturbance intends to simulate a point of contact of the drill string with the well walls, something that is common in operations, specially when non-vertical well are being digged. This friction was positioned at half length of the reduced scale drill string model.

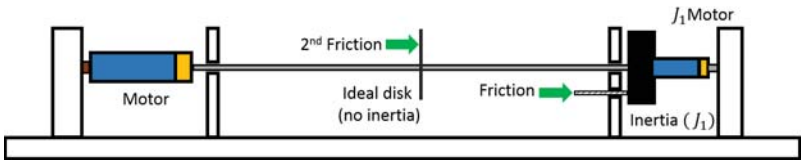

Figure 3.19: Mechanical model with second dry friction point

For this simulations a L_1 control was used with the following reference system:

$$A = \begin{bmatrix} 0 & 1 & 0 \\ 0 & \frac{-C_m}{(J_m+J_1)} & \frac{K_t}{(J_m+J_1)} \\ 0 & \frac{-K_t}{L_{DC}} & \frac{-R_{DC}}{L_{DC}} \end{bmatrix} \quad B = \begin{bmatrix} 0 \\ 0 \\ \frac{0.1}{L_{DC}} \end{bmatrix} \quad x = \begin{bmatrix} \theta \\ \dot{\theta} \\ i \end{bmatrix} \tag{3.33}$$

where the state space equations are in the form:

$$\dot{x} = Ax + Bu \tag{3.34}$$

This system is a 2 DOF model of a DC motor with an inertia (J_1) connected directly to the motor inertia (J_m), where K_t is the torque constant and R_{DC} and L_{DC} are the motor electrical resistance and inductance.

This system is then transformed to a transfer function representation using the parameters from table 3.1, after removing a pole-zero pair in the transfer function.

Parameter	**Value**	**Unit**
Motor Viscous friction (C_m)	1.784×10^{-4}	kgm^2/s
Moment of inertia of motor (J_m)	0.37×10^{-3}	kgm^2
Armature inductance (L_{DC})	1.10×10^{-3}	H
Armature resistance (R_{DC})	0.33	Ω
Torque constant (K_t)	0.12	Nm/A
Speed constant (K_e)	6.02×10^{-2}	$V/(rad/s)$

Table 3.1: Model parameters

$$M(s) = \frac{376.3}{s^2 + 391.1s + 349.8} \tag{3.35}$$

And the low pass filter $C(s)$:

$$C(s) = \frac{20^4}{(s+20)^4} \tag{3.36}$$

Figure 3.20 shows the reference system (3.35) response to step of amplitude $20rad/s$.

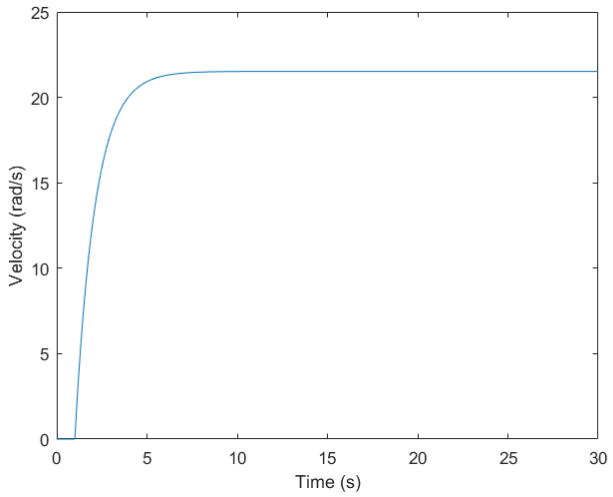

Figure 3.20: Reference system response to a step at $T = 1s$ with amplitude of 20

Figure 3.21 shows the bode plot of the $C(s)$ filter. It is a low pass filter with $-3dB$ frequency of 8.68 rad/s and unitary gain on the pass band.

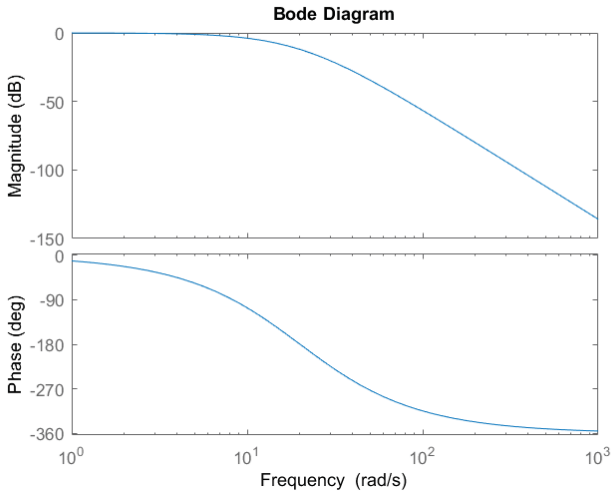

Figure 3.21: Magnitude and phase plot of the $C(s)$ filter

As one can note, the step response is slow due to the high inertia to motor-power ratio, and no overshoot is present. It is also notable that this system has a DC gain slightly different from 1, being $DC_{gain} = 1.0760$

The PID response for this system is shown in fig. (3.22). The system was simulated in open loop from $T = 0$ to $T = 10s$. Then the PID controller is turned ON and tries to stabilize the speed at 10 rad/s. Table 3.2 shows the gains of the PID controller.

Parameter	Value
Proportional gain (P)	8.0468
Integral gain (I)	31.6684
Derivative gain (D)	1.3682

Table 3.2: PID gain

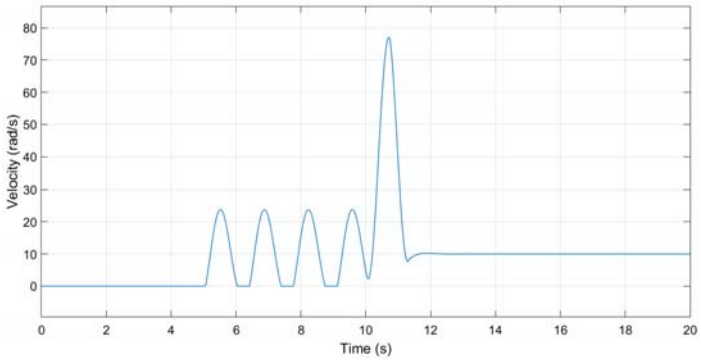

Figure 3.22: Angular velocity response of PID control

As one can note, the stick slip is very severe in the system without control (before T=10s), there is a lot of overshoot when the control is turned on, and the settling time is very high.

The L_1 control for this case, has a result even further away from what is desirable as fig. 3.23 shows.

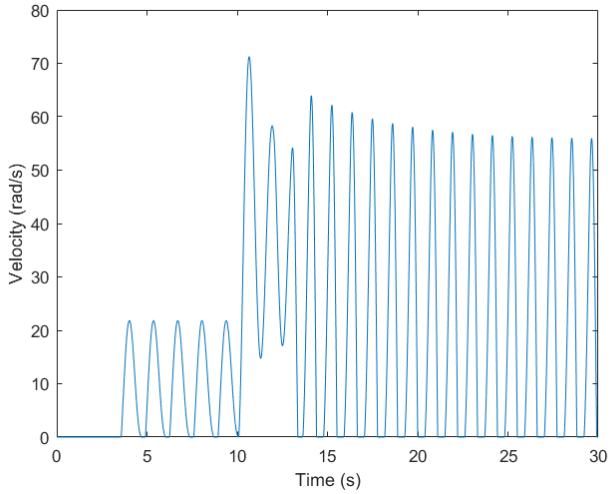

Figure 3.23: L_1 control system response

The result for this L_1 implementation actually makes the system even worse, the stick-slip is still present but now with a larger amplitude.

Implementing the L_1 augmented control strategy proposed, a much better result is obtained, the overshoot is smaller than the expected in PID, and the

oscillations are also smaller.

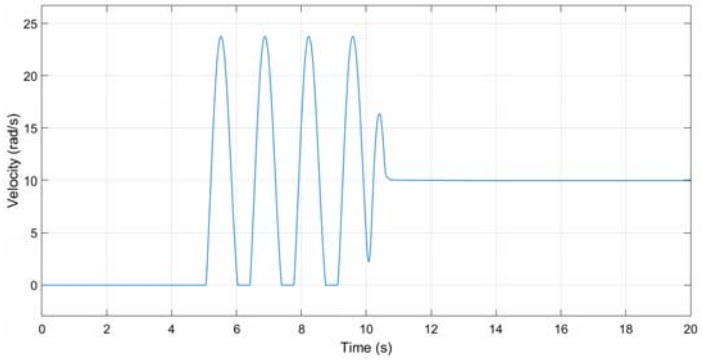

Figure 3.24: PID augmented L_1 controller response

Figure 3.24 shows the system response of the PID augmented L_1 control. The control is again turned on at T=10s, after the system has established a stick-slip behavior. The Control, can then mitigate the oscillations in a short period and smoothly bring the system to the set point.

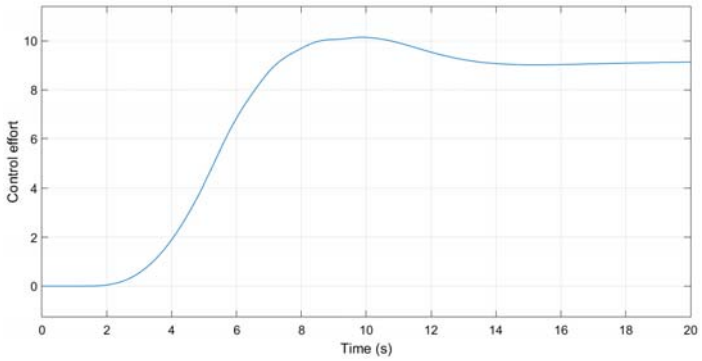

Figure 3.25: PID augmented L_1 controller control effort

Figure 3.25 shows the control effort of the L_1 in this simulation. The contol effort is shown from T=0, but it is not being fed into the system before T=10s.

In the case where the control is ON since $T = 0s$, we can observe a much better response of the system controlled by PID, as the time delay added on the measurement of J_1 is not much important in the beginning. Figure 3.26 shows the result of the PID for this case.

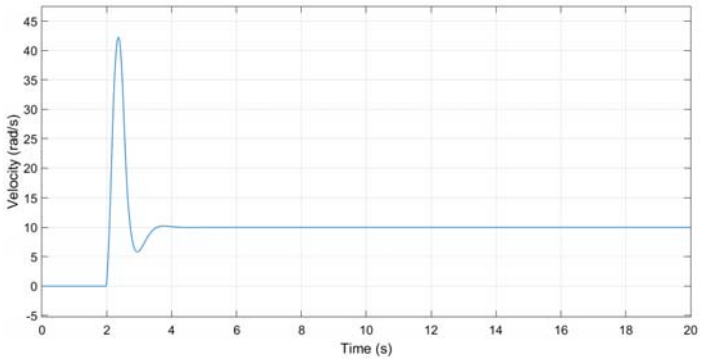

Figure 3.26: PID controlled system response

One can note that there is a severe overshoot in the response, but the system is stabilized effectively. Again, L_1 control alone has an unstable behavior (fig.3.27) and therefore no applicability on this problem.

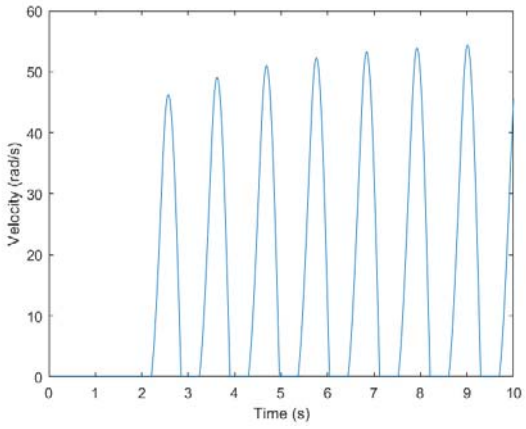

Figure 3.27: L_1 controlled system response

Just as the previous case, the use of the PID augmented L_1 controller, has an even better result when applied since the beginning of the test.

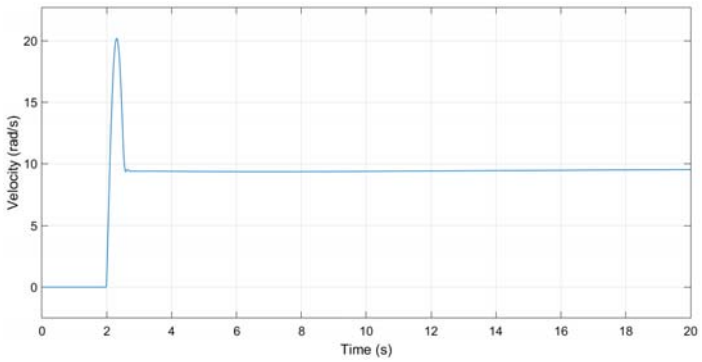

Figure 3.28: PID augmented L_1 controller response

Figure 3.28 shows the result of this simulation. One can note that the overshoot of the velocity in J_1 response comes from above 40 rad/s in the case of the PID controller to around 20 in the case of the augmented L_1 controller, noting that the reference signal to be tracked is 10 rad/s.

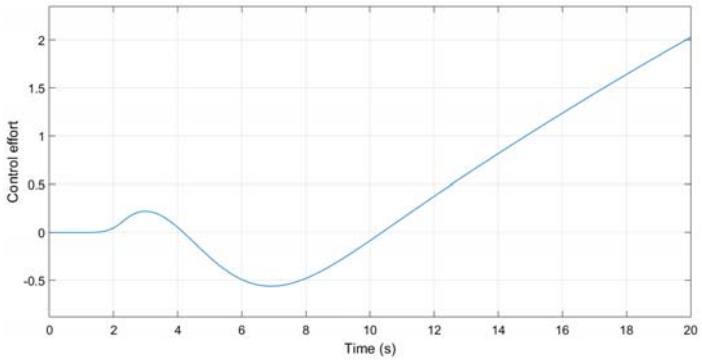

Figure 3.29: PID augmented L_1 controller control effort

Figure 3.29 plots the control effort of the L_1 augmented control.

Next, the time delay described in fig. 3.18 is increased from 20ms to 40ms to test the time delay margins of the system. The system operates in open loop until $T = 10s$, when the controller is turned on to reduce the stick-slip. Figure 3.30 shows the result of the angular velocity of J_1 for this simulation. One can note that the time delay on the output measurement induces a small amplitude steady state oscillation on the system.

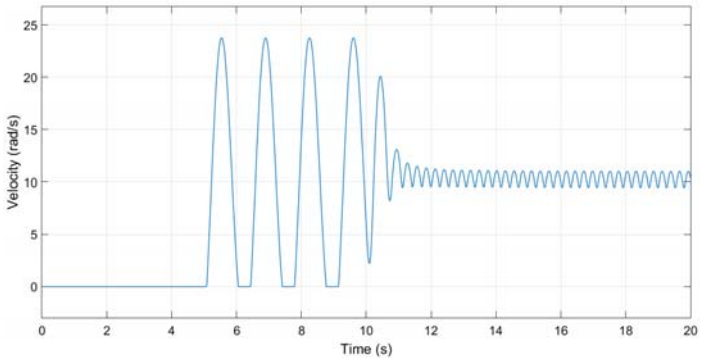

Figure 3.30: PID augmented L_1 controller response with 40ms time delay

The PID controller with the same 40ms time delay (fig. 3.31) shows the same steady state small amplitude oscillations and the large overshoot when the controller is turned on at $T = 10s$.

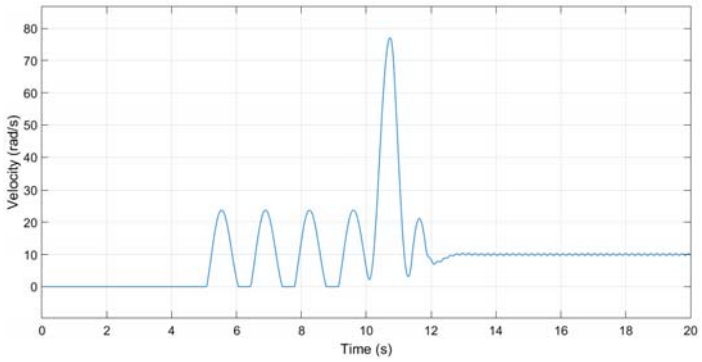

Figure 3.31: PID augmented L_1 controller response with 40ms time delay

In both cases (PID and L_1) the controllers eliminated the stick-slip, even with a 40ms time delay present in the output measurement. The oscillations of the system indicate that the controllers are close to the time delay margins for this case.

3.7 Multi-Objective Filter Optimization for Output Feedback L_1 Adaptive Controller

As the filter $C(s)$ is the most challenging part of the L_1 structure to be designed and tuned, there are still many divergences and proposed methods to design and tune this low pass filter. Formulation presented in section 3.4, the one used up to this point, shows a good result, but novel techniques aim to improve the response of the L_1 controller by better tuning the $C(s)$ low pass filter.

In the most recent and most promising article in this line, Hamidreza [20] presents a Convex Multi-Objective filter optimization for output feedback in L_1 adaptive controller, and therefore this section is based on this proposed methodology and presents the results of using this multi-objective optimization on the drilling problem object of this thesis.

One of the main advantages of L_1 adaptive control architecture, presented in section 3.4, is that the estimation loop is decoupled from the control law. This decoupling allows for the use of arbitrary fast estimation rates, leading to uniform performance bounds and guaranteed robustness in the presence of nonlinearities and uncertainties. As a result, the closed-loop system converges to the reference system, which is linear, and hence has a scalable, repeatable, and predictable response.

This decoupling in the L_1 adaptive control architecture, is achieved by a low-pass filter $C(s)$, which attenuates high-frequency signals resulting from the

fast estimation. The filter design is therefore critical for the trade-off between performance and robustness of the closed-loop system.

The optimal filter design can be obtained by formulating the problem as a constrained optimization problem. In addition to the robust stability condition, we define the performance criteria for trade-off of robust stability and robust performance.

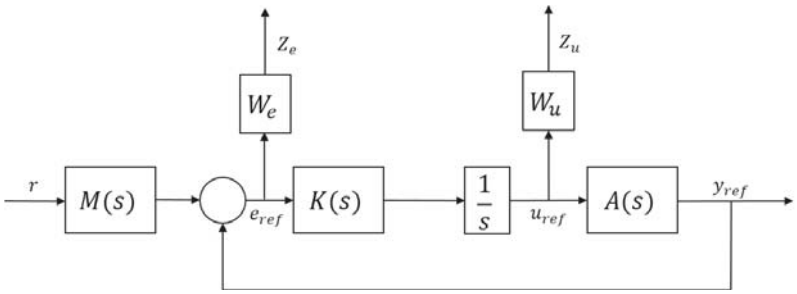

Figure 3.32: Simplified output feedback system

Figure 3.32 shows an output feedback system where the signals Z_e and Z_u are the performance outputs. The signal Z_e is the weighted error signal between the desired system output and the actual reference output y_{ref} . $W_e(s)$ is the weight function on the error signal which is chosen based on tracking performance requirements. The other performance measure, Z_u, is the weighted control input as shown in fig. (3.32). $W_u(s)$ is the weight function on the control input. By minimizing the norm defined for weighted control input in the cost function, we can reduce undesirable control actuation. In this case, we minimize the H_2-norm of the transfer functions from reference input r to the performance output signals Z_e and Z_u. Minimizing the H_2-norm ensures zero steady-state tracking which corresponds to DC-gain condition for the filter design ($C(0) = 1$).

Considering:

$$K(s) = \frac{sC(s)}{(1 - C(s))M(s)} \tag{3.37}$$

and

$$T(s) = f_l(f_u(G(s), \Delta(s)), K(s)) \tag{3.38}$$

where f_u and f_l denote linear upper and linear lower fractional transformations, respectively. A combination of a mixed L_1/H_2 cost-function and L_1 robust stability constraint ensures uniform bound on transient response

and zero steady-state error. Therefore, the constrained optimization problem for filter design is proposed as follows:

$$inf_{K(s)} \quad ||T_{44}(K(s))||_{H_2}^2 + ||T_{45}(K(s))||_{H_2}^2 + c||T_{11}(K(s))||_{L_1} \tag{3.39}$$

subject to:

$$||\Psi(K(s))||_{L_1} < 1 \tag{3.40}$$

where T_{ji} is a mapping from the input w_i (i^{th} element of input vector) to the output v_j. In this formulation, the L_1-norm constraint ensures stability of the closed-loop system in the presence of three sources of uncertainties (delay, input nonlinearities and disturbances, and system parametric uncertainties). Depending on the specific problem, if some of the uncertainties are not present, the mapping can be reduced to a lower dimensional system.

In order to optimize the filter, it is necessary to obtain a reference model of the system that presents the closest representation of the behavior of the plant as possible. In this case a 2DOF mechanical system with addition of the DC motor dynamics was chosen. This reference model is obtained based on a simplification of the actual plant we intend to control.

$$A = \begin{bmatrix} 0 & 1 & 0 & 0 & 0 \\ 0 & \frac{-K}{J_m} & \frac{-(C_m+D_{il})}{J_m} & \frac{K}{J_m} & \frac{K}{J_m} \\ 0 & 0 & 0 & 1 & 0 \\ \frac{K}{J_1} & \frac{D_{il}}{J_1} & \frac{-K}{J_1} & \frac{-D_{il}}{J_1} & 0 \\ 0 & 0 & 0 & \frac{-K_e}{L_{DC}} & \frac{-R_{DC}}{L_{DC}} \end{bmatrix} \quad B = \begin{bmatrix} 0 \\ 0 \\ \frac{1}{J_m} \end{bmatrix} \quad x = \begin{bmatrix} \theta_m \\ \dot{\theta_m} \\ \theta_1 \\ \dot{\theta_1} \\ i \end{bmatrix} \tag{3.41}$$

When comparing the step response of this system (fig. 3.33) with the one composed only by the motor attached directly to the inertia (fig. 3.20), one can note the characteristic oscillation that comes from the addition of the torsional spring between the motor inertia (J_m) and the inertia disk (J_1)

By solving the proposed equations to optimize the filter we obtain equation (3.42) for the low pass filter.

$$C(s) = \frac{0.000918s^3 + 0.03327s^2 + 0.5077s + 0.1127}{s^4 + 5.884s^3 + 24.81s^2 + 5.903s + 0.1127} \tag{3.42}$$

Figure 3.34 shows the bode plot of the optimized filter (3.42). We note that is a 4^{th} order low pass filter with $-3dB$ frequency of $0.021rad/s$ and

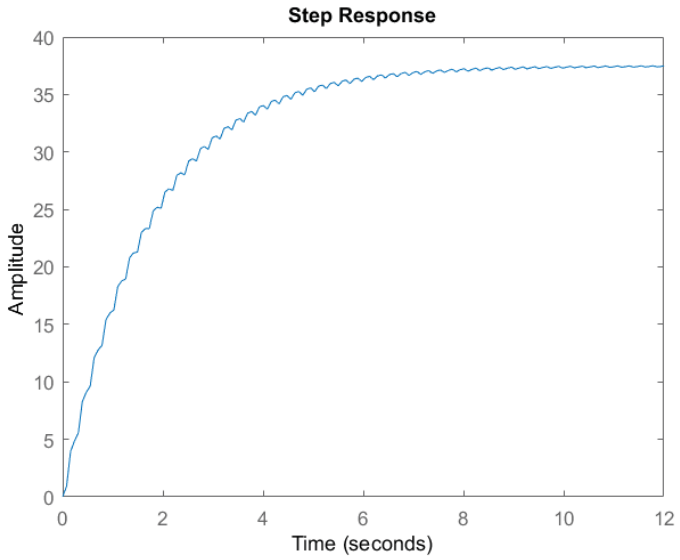

Figure 3.33: Step response of the reference system

unitary gain on the pass band as it should be.

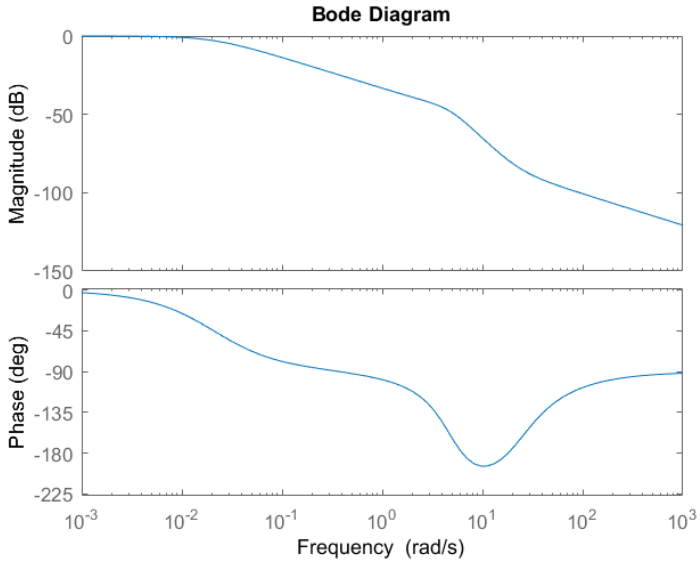

Figure 3.34: Bode plot of the optimized low pass filter

The optimized L_1 augmented controller, turned on at $t = 10s$, after the beginning of the stick slip phase, shows a very good response, there is almost no oscillations after the control is turned on, stabilizing the angular velocity of J_1 at 10 rad/s. Simulations are performed with the addition of a second dry friction point acting on half length of the drill string and a $20ms$ time delay on the measurement of the output (i.e. velocity of J_1) as shown in fig. 3.18.

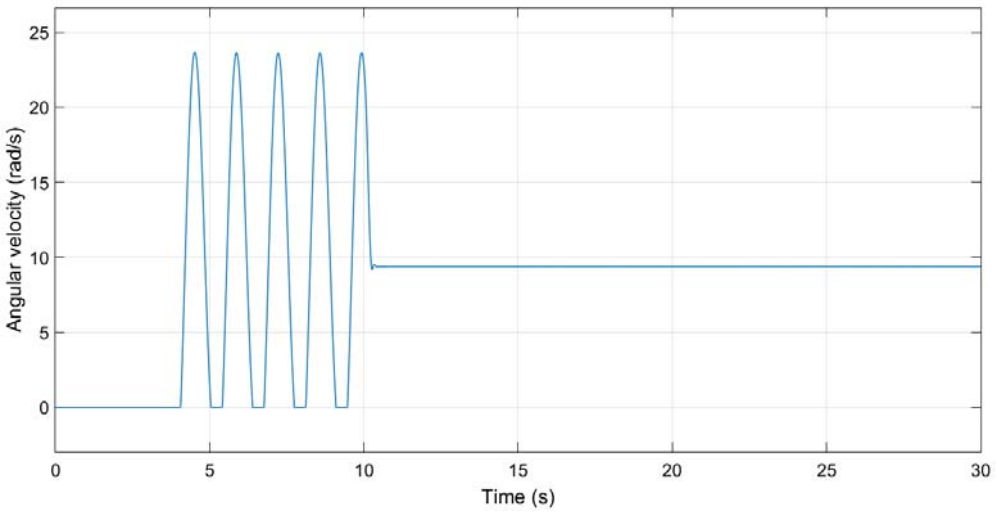

Figure 3.35: L_1 control system after optimization

Figure 3.35 shows the angular speed of J_1 over time for the optimized L_1 control. The advantages of this proposed optimized L_1 controller become very clear when we compare the result with the ones obtained simulating the same system controlled by a well tunned PID controller, as shown in fig. 3.36.

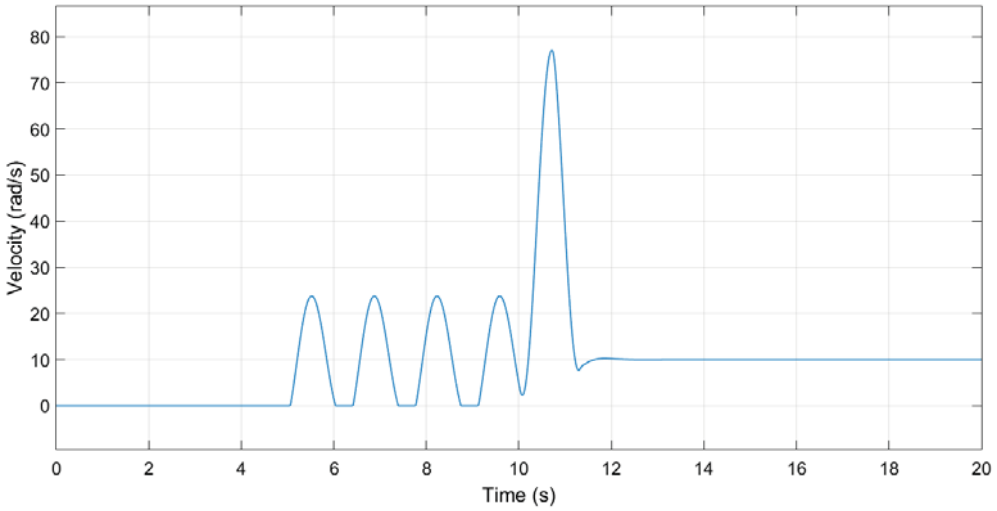

Figure 3.36: PID controlled system

One can see that the maximum amplitude of the overshoot in the velocity of J_1 is around 70 rad/s, more than 4 times bigger than the desired speed of 10 rad/s. And the settling time on this control is around 6s versus around 1s on the L_1 control case (i.e. 6 times bigger). This bad performance of the PID is expected, specially for systems with considerable time delays, as this case.

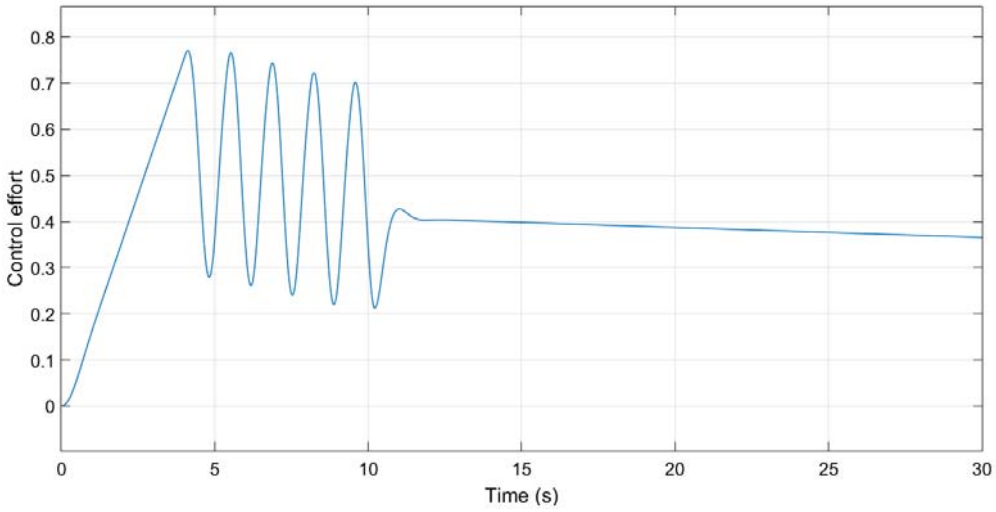

Figure 3.37: Control effort of the optimized L_1 controller

Figure 3.37 shows the control effort of the L_1 augmented control, confirming that little adaptation is needed in this case.

If we consider the same system but with the L_1 control starting from T=0s L_1 control is still able to control the system with an overshoot similar to the one experienced when turning the control on at T=10s (fig.3.35).

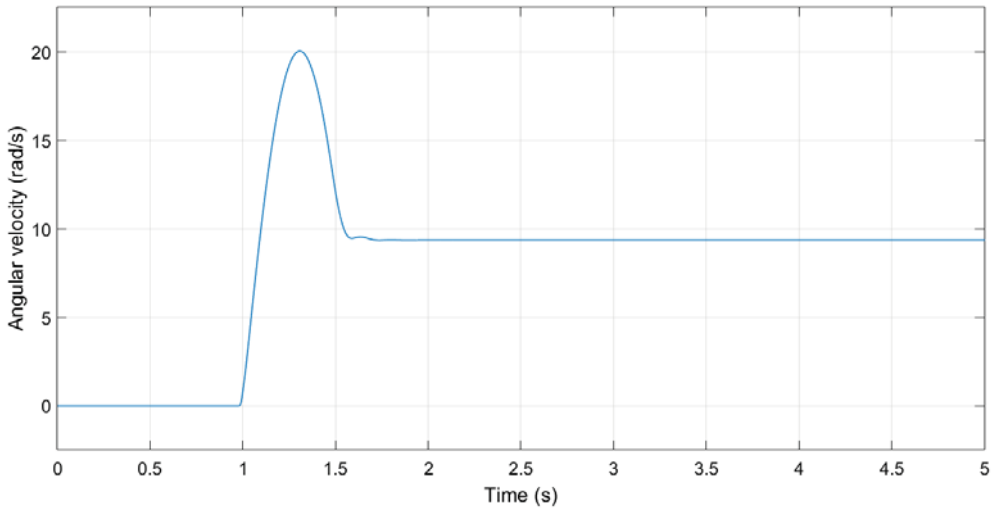

Figure 3.38: L_1 control system after optimization starting at T=0s

The PID response in this case (fig. 3.39) is much better than the one with the control turned on at T= 10s (fig. 3.36). This occurs as starting the control since the beginning on a steady state system the 20ms time delay applied on the output has a reduced influence on the overall performance of the system. The settling time and the overshoot are much smaller in this case.

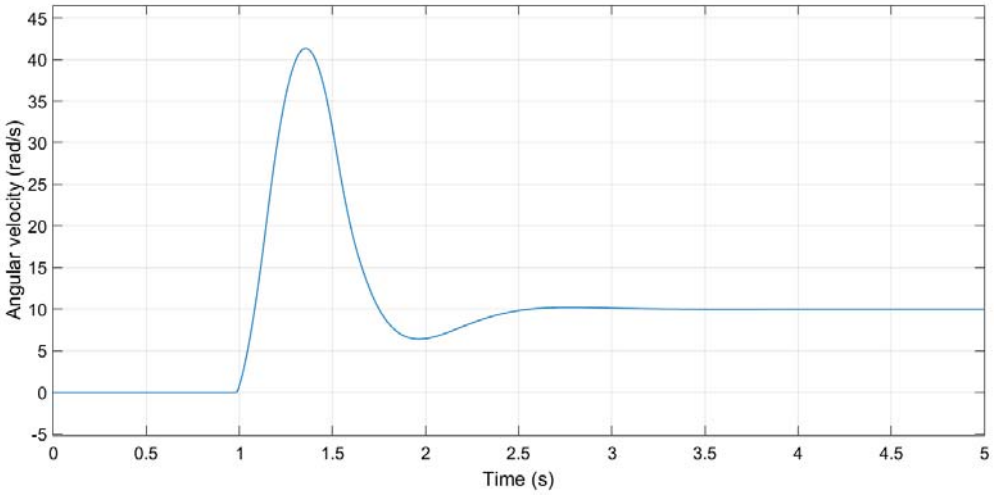

Figure 3.39: PID controlled system starting at T=0s

From the simulations presented in this section one can note that the design of the low pass filter $C(s)$ of the L_1 adaptive controller has a big influence on its results. Despite there is still not yet in literature a best method to design the filter, the method from Hamidreza [20] used in this section provides good results in the problem of the drillstring studied in this thesis.

In the next chapter, the experimental setup of a torsional system is described, its components, mechanical characterization and in the end, an experimental and mathematical methodology for stick-slip avoidance based on the dynamical behavior of the system is presented.